

# Atmospheric pressure loading for routine data analysis

Leonid Petrov

NVI/NASA Goddard Space Flight Center, Greenbelt, Maryland, USA (Leonid.Petrov@gsfc.nasa.gov)

Jean-Paul Boy

NASA Goddard Space Flight Center, Greenbelt, Maryland, USA (boy@bowie.gsfc.nasa.gov)

**Abstract.** We have computed 3-D displacements induced by atmospheric pressure loading from 6-hourly surface pressure field from NCEP (National Center for Environmental Predictions) Reanalysis data for all Very Long Baseline Interferometry) and SLR (Satellite Laser Ranging) stations. We have quantitatively estimated the error budget our time series of pressure loading and found that the errors are below 15%. We validated our loading series by comparing them with a dataset of 3.5 million VLBI observations for the period of 1980–2003. We have shown that the amount of power which is present in the loading time series, but does not present in the VLBI data is, on average, only 5%. We have also succeeded, for the first time, to detect horizontal displacements caused by atmospheric loading. The correction of atmospheric loading in VLBI data allows a significant reduction of baseline repeatability, except for the annual component.

## 1 Introduction

Atmospheric pressure variations which can reach 50 mbar induce deformation of the solid Earth at the level of several centimeters, which certainly should be taking into account in routine analysis of space geodesy observations. Atmospheric loading effects are computed by convolving the surface pressure field with Green's functions (see, for example, Farrell (1972)).

van Dam and Herring (1994) and van Dam et al. (1994) have computed atmospheric loading using a former atmospheric model from the NMC (National Meteorological Center) with  $2.5$  by  $2.5$  spatial resolution and 12 hour sampling and applied to VLBI (Very Long Baseline Interferometry) and GPS (Global Positioning System) site position data. Analysis of reduction of variance of baseline lengths showed that atmospheric loading signal was clearly present

in VLBI and GPS datasets. However, only 62% of the power of the signal computed using their model was found in the VLBI data. This unexplained discrepancy and very high computational cost of pressure loading calculation are the reasons why modeling atmospheric pressure loading computed using the global numerical weather model did not come into practice of routine data analysis.

There are several reasons which motivated us to re-visit this topic: the accuracy of VLBI geodetic observations has increased during the last ten years which has improved our ability to detect tiny crustal motions. The NCEP/NCAR (National Center for Environmental Predictions / National Center for Atmospheric Research) Reanalysis project (Kalnay et al. (1996)) provides us a continuous and uniform dataset of surface pressure with a 6 hour temporal resolution on a  $2.5$  by  $2.5$  grid for the period 1948–now. Because of the computer and network improvements, it is now possible to compute on a operational basis the series of the atmospheric loading and apply them in a routine data analysis process, for example, for the Earth orientation service.

In section 2, we describe our model of the atmospheric pressure loading and present the error budget of the loading time series. In section 3, we validate the time series of site displacements induced by pressure loading by re-analyzing a dataset of 3.5 million of VLBI observations for the period 1980–2003. We have estimated global admittance factors for vertical and horizontal components. We also computed the reduction of variance of baseline lengths in order to compare our results with van Dam and Herring (1994). Discussion and concluding remarks are given in section 5. Brief outlines of the atmospheric pressure loading service are given in section 6.

## 2 Computation of atmospheric pressure loading

### 2.1 Characteristics of atmospheric pressure loading

Displacements at the Earth’s surface induced by surface pressure loading are computed by convolving Green’s functions (Farrell (1972)) with the surface pressure field from NCEP Reanalysis (Kalnay et al. (1996)).

We model the ocean response to pressure forcing as the inverted barometer (IB). It has been shown that this model is adequate for describing sea height variations for periods typically longer than 15–20 days (see, for example, Wunsch and Stammer (1997)). However the ocean response to atmospheric pressure forcing significantly deviates from the IB hypothesis at higher frequencies (Tierney et al. (2000)). We also assume that enclosed and semi-enclosed seas respond to atmospheric pressure as a ”non-inverted barometer”, i.e. pressure variations are fully transmitted to sea floor.

Figure 1 and 2 shows the time series and their power spectrum for the period 2000–2003 at the Hartrao and Wetzell stations. They are representative of mid-latitude and equatorial inland stations.

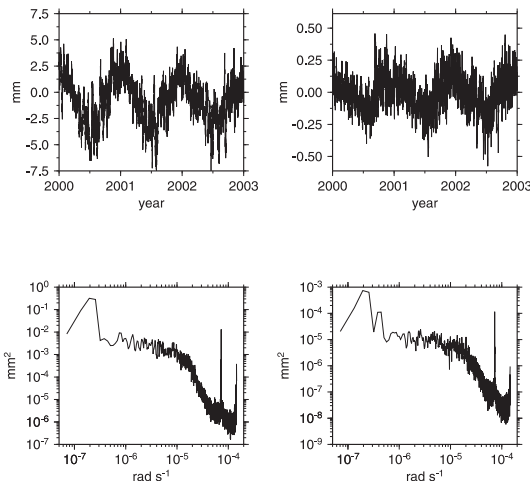


Figure 1: Vertical (left) and north (right) displacement induced by atmospheric loading for Hartrao station.

All station displacements show significant narrow-band diurnal ( $S_1$ ), semidiurnal ( $S_2$ ) and annual ( $S_a$ ) signals. Displacements for low-latitude stations are characterized by a strong

wide-band annual and semi-annual signal and relatively weak amplitudes for periods below 10 days (except the  $S_1$  and  $S_2$  peaks).

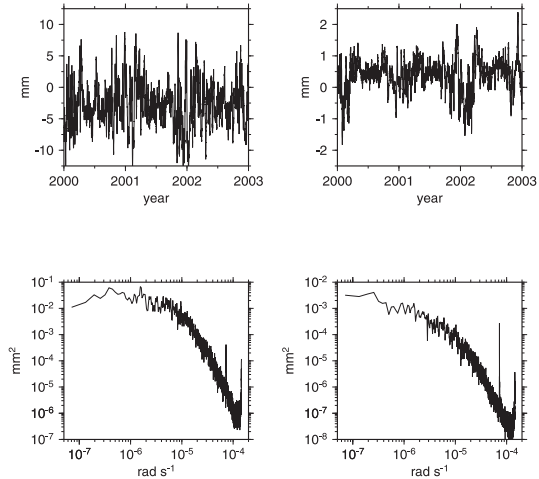


Figure 2: Vertical (left) and east (right) displacement induced by atmospheric loading for Wetzell station.

Mid latitude stations show the opposite behavior; the mid-latitude atmospheric circulation is determined by the circulation of low and high pressure structures with typical period of 5–10 days. These periods are also the limit of the validity of the IB assumption.

### 2.2 Error budget

We would like to quantitatively assess the error budget of our atmospheric loading series. We identified four major sources of errors: 1) errors in the Green’s functions, 2) errors in the surface pressure field, 3) errors in the land-sea mask and, 4) mismodeling of the ocean response to pressure forcing.

The Green’s functions are computed for a spherically symmetric, non rotating, elastic and isotropic (SNREI) Earth model, adopting PREM (Dziewonski and Anderson (1981)) elastic parameters. Therefore, we neglect the effects induced by Earth’s anelasticity and ellipticity. The differences between our Green’s functions and Green’s functions for an anelastic Earth model (see, for example, Pagiatakis (1990)) are typically below 1-2%. The effect induced by the Earth’s ellipticity is of the order of magnitude of the Earth’s flattening, i.e. 0.3%.

Another source of possible errors is the errors in the surface pressure field from NCEP Reanaly-

sis. The first way to estimate them is to compare NCEP pressure field with ground pressure measurements. Velicogna et al. (2001) compared the differences between this atmospheric model and direct barometric observations. We would like to quantitatively assess the error budget, but since the spatial coverage of barometric measurements is not homogeneous, we choose another way to characterize possible errors, and we estimated the differences between two NCEP numerical weather models: NCEP Reanalysis and NCEP Operational Final Analysis. We have computed the station displacements with the NCEP Operational surface pressure field with a spatial resolution of  $1^\circ 0$ . The RMS of the differences between the 3-D displacements computed with both pressure fields is, on average, about 10%. However, these differences are larger in mountainous areas; this is due to the fact that the  $2^\circ 5$ , or even the  $1^\circ 0$  spatial resolution of the NCEP Reanalysis and NCEP Operational datasets is not sufficient to model the topography in mountainous areas and, therefore, the surface pressure variations.

Since the  $2^\circ 5$  resolution of the NCEP Reanalysis data is not sufficient to correctly represent the coastline, we choose a land-sea mask with a  $0^\circ 25$  resolution derived from FES99 (Lefèvre et al. (2002)) ocean tidal model. In order to estimate the errors induced by the land-sea mask, we have computed 3-D site displacements with two land-sea masks with  $0^\circ 25$  and  $0^\circ 50$  resolution. The differences between the two time series do not exceed 5%. However the differences between the loading estimates with the  $2^\circ 5$  and  $0^\circ 25$  land-sea masks can reach 10% for the vertical components and for the 30% horizontal components, even for an inland station like Wettzell (Germany) 500 km far from the coasts.

In order to estimate the errors induced by the mismodeling of the ocean response to pressure at high frequency, we compared ocean bottom pressure variations, as well as the induced loading effects, from two runs of the CLIO (Coupled Large-scale Ice Ocean) global circulation model (Goosse and Fichelet (1999)). The first run is forced by atmospheric pressure, surface winds and heat-fluxes (de Viron et al. (2002)), and the other one is forced only by winds and heat-fluxes, i.e. assuming an IB response. The differences between these two runs are, therefore, interpreted as the departure of the ocean response to pressure forcing to the IB hypothesis. We have found that the mean vertical and horizontal dif-

ferences are respectively below 10% and 20%. As expected these differences can be larger for island stations or stations close to the coast.

Table 1: Global error budget of atmospheric loading estimates.

Error source	rms
Green's functions	2 %
Surface pressure field	10 %
Land-sea mask	5 %
Ocean response	10 %
Total	15 %

Table 1 gives a summary of the global error budget. Combining all sources of errors, we can evaluate the uncertainty of the site displacements induced by atmospheric pressure loading at 15%.

### 3 VLBI data processing

#### 3.1 VLBI data processing

The processing of VLBI observations of time delays mostly follows the procedure described and Sovers et al (1998) and outlined in the IERS Conventions (McCarthy, 1996). Semi-empirical IERS96 nutation expansion was used. We modeled ocean tidal loading with GOT00 (Ray (1999)) model for diurnal and semi-diurnal waves, NAO99 (Matsumoto et al. (2000)) model for long-period zonal waves, and equilibrium tide for the polar tides and 18.6 year wave. NMF Mapping functions developed by Niell (1996) were used for modeling tropospheric path delay.

#### 3.2 Analysis of global admittance factor

In solution G1 we computed admittance factors of the vertical, east and north components of the atmospheric pressure loading time series displacements into VLBI time delay, averaged over all sites.

These admittance factors entered the estimation model the following way:

$$\tau = \sum_{i=1}^3 A_{i1} a_{i1} \frac{\partial \tau}{\partial r_{i1}} - A_{i2} a_{i2} \frac{\partial \tau}{\partial r_{i2}} + \dots \quad (1)$$

where  $\tau$  is VLBI time delay,  $a_{ij}$  is the topocentric vector of the modeled site displacements due to atmospheric pressure loading for the  $j$ th station,  $r_{ij}$  is the topocentric site coordinate vector. The index  $i$  runs through up, east and north components of the topocentric radius-vector. The

unknown vector of the admittance factors  $A$  was estimated in a single weighted LSQ fit together with site position and velocities, source coordinates, Earth orientation parameters (EOP) as well as 1.2 million nuisance parameters.

It can be shown that these admittance factors can be interpreted as correlation coefficients between the true (unknown) site displacements and our loading estimates within the validity of the assumption that the time series of the modeled site position displacements caused by atmospheric pressure loading and unmodeled contribution to time delay are *not correlated*. We refer the reader to Petrov and Boy (2003) for more details.

We performed 4 different solutions. In solution G1 we treated the three-dimensional vector of the admittance factor as a global parameter, which is common for all sites. Then we passed the time series of the site position variations through a narrow-band filter and extracted the annual component of the pressure loading signal. In the solution G2 we estimated admittance factors for these time series. In the solution G3 we estimated the admittance factor to the atmospheric pressure loading series with the annual component filtered out. Results are presented in Table 2. We also performed another solution in which we estimated admittance factors for each individual station.

The estimates of the admittance factors of the time series of atmospheric pressure loading with removed annual component are closer to unity. Annual signals in site positions may be induced by other unmodeled signals such as hydrologic loading or thermal antenna height deformation (Nothnagel et al. (1995)) which are not modeled in this study. For example, van Dam et al. (2001) showed, that the contribution of continental water loading can reach several cm at seasonal time scales.

Contrary to wide-band signals, independent narrow-band signals are almost always correlated. Thus, condition of validity of this test is violated when we consider the annual signal.

Table 2: Global Admittance Factors from VLBI solutions.

Solution	Up	East	North
G1	$0.95 \pm 0.02$	$1.16 \pm 0.06$	$0.84 \pm 0.07$
G2	$0.46 \pm 0.09$	$1.08 \pm 0.26$	$-0.89 \pm 0.26$
G3	$0.98 \pm 0.02$	$1.21 \pm 0.06$	$1.02 \pm 0.07$

Although the mean admittance factors are very close to unity, the admittance factors for individual stations are not always close to unity. We can often link anomalous admittance with the site positions. Stations located in mountainous areas or in the vicinity of the oceans are usually characterized by low admittance factors, even sometimes negative values. This can be explained, as we showed in section 2.2, by errors in the atmospheric pressure field on mountainous areas and errors induced by the mismodeling of oceanic response to atmospheric pressure loading.

### 3.3 Analysis of reduction of variance coefficients

In order to compare our results with results of van Dam and Herring (1994), we made another three solutions; in solution B1, we did not apply the atmospheric loading contribution, but we did it in the solution B2. In solution B3 we have applied the contribution of the atmospheric pressure loading time series with the annual component filtering out.

We used the reduction of variance coefficient  $R$  of baseline lengths as a measure of agreement of the atmosphere pressure loading displacements series with observations:

$$R = \frac{\Delta\sigma^2 + \sigma_m^2}{2\sigma_m^2} \quad (2)$$

where  $\Delta\sigma^2$  is the difference between the mean square of baseline length residuals before and after adding the contribution due to station displacements caused by the atmospheric pressure loading, and  $\sigma_m$  is the variance of the atmospheric loading.

A linear model was fitted in the series with discontinuities at epochs of seismic events for several stations. The weighted root mean square of residual baseline lengths was computed for all baselines with more than 100 sessions for B1, B2 and B3 solutions. 69 baselines fitted this criterion. The coefficients of reduction of variance were computed using baseline length variances. The mean coefficient of reduction of variance of the B2 solution with respect to the reference solution B1 is  $0.86 \pm 0.04$ . The mean coefficient of reduction of variance of the B3 solution with respect to the reference solution B1 is  $0.92 \pm 0.04$ .

Van Dam and Herring (1994) found a reduction of variance of  $R = 0.62$  and  $R = 0.76$  with-

out the annual component. Our estimates are significantly closer to unity than theirs. We attribute these difference partly to improvements in modeling atmospheric loading, and partly to improvements of geodetic observations. Van Dam and Herring used an older atmospheric model provided by NMC (National Meteorological Center) with the same spatial resolution and a 12 hour temporal sampling compared to the 6-hours for the NCEP Reanalysis model. The NCEP Reanalysis is also a uniform and continuous dataset, whereas the NMC pressure field had several discontinuities related to changes in the model. We used a land-sea mask with a higher resolution ( $0.25^\circ$ ) for modeling the IB response.

#### 4 Discussion and Conclusion

A priori estimates of the errors of our time series of the site displacements induced by atmospheric pressure loading are less than 15%. The estimates of the admittance factors from the solution G1 demonstrate that on average 95% of the power of the modeled pressure loading signal presents in the data well within the error budget. It allows us to make an important conclusion that in average our model of the atmospheric pressure loading *quantitatively* agrees with observations. The existence of the significant discrepancy between the model of the displacements caused by the atmospheric pressure loading and observations reported by van Dam and Herring (1994) has not been confirmed. Except for the annual component, applying the atmospheric loading model results in a reduction of the power of the residual harmonic site position variations. For the first time we have detected horizontal component of atmospheric pressure loading in VLBI observations.

Although we have an excellent agreement between the model of atmospheric pressure loading and the observations in average, the estimates of the admittance factors significantly deviate from unity for some individual stations, suggesting deficiency of the model for these sites. These stations are located either close to the coastline or in mountainous regions. In the first case, improvement of atmospheric loading modeling requires to model the high-frequency ocean response to pressure forcing which significantly deviates from the IB assumption. In the other case, the spatial resolution of NCEP Reanalysis data ( $2.5^\circ$ ) is too coarse to model the topography and therefore at-

mospheric pressure variations.

We evaluate the effects of modeling atmospheric loading on EOP estimation. We made two solutions, one with applying the contributions of the 3-D atmospheric loading displacements, the other without. The RMS differences in polar motion and the UT1 angle between these two solutions are typically about 100 prad, which is 2–4 smaller than the current EOP uncertainties.

#### 5 Service of the atmospheric pressure loading displacements

The tests described above allowed us to make a conclusion that the model of the atmospheric pressure loading has passed validation tests. We have computed continuous atmospheric pressure loading series for all VLBI and SLR sites starting from 1976.05.05. We found that when the atmospheric pressure loading series are computed for two sites separated by  $0.05^\circ$ , the differences in site displacements never exceed the 1% level. Therefore, in the case if several VLBI or SLR stations are located within 3 km from each other, the atmospheric pressure loading was computed only for one station and considered common for all stations located within this site.

The first epoch of the atmospheric pressure loading time series is three days before the first observation used in data analysis and the last epoch is three days after the last observation of the site in the case if all stations at the site has ceased operations. Thus, these epochs are different for each site.

The series of the atmospheric pressure loading for the sites, which are considered as active, i.e. continuing observations, are updated every day. The file with surface pressure from the NCEP Reanalysis for the last year is retrieved by ftp, split into monthly sections and stored. The atmospheric pressure loading time series for active sites are augmented if the surface pressure files contain data for the epochs for which the pressure loading has not been computed. The NCEP Reanalysis numerical weather model are updated daily with the time lag 3–7 days. Our atmospheric pressure loading time series also updated with the time lag 3–7 days.

Starting from December 2002 the atmospheric pressure loading contribution is incorporated in the model of VLBI data reduction in all solutions of the Goddard VLBI group, including

operational EOP solutions. The atmospheric pressure loading time series are available on the Web at <http://gemini.gsfc.nasa.gov/aplo/> for all everybody without restrictions.

## References

- de Viron, O., H. Goosse, C. Bizouard and S. Lambert (2002). High-frequency non-tidal effect of the ocean on the Earth's rotation, *EGS 27th General Assembly*. Nice, France.
- Dziewonski, A.M. and D.L. Anderson (1981). Preliminary Reference Earth Model. *Phys. Earth Planet. Inter.*, 25, pp. 297–356.
- Farrell, W.E. (1972). Deformation of the Earth by surface loads. *Rev. Geophys. Space Phys.*, 10, pp. 751–797.
- Goosse, H. and T. Fichelet (1999). Importance of ice-ocean interactions for the ocean circulation: a model study. *J. Geophys. Res.*, 104, pp. 23,337–23,355.
- Kalnay, E., M. Kanamitsu, R. Kistler, W. Collins, D. Deaven, L. Gandin, M. Iredell, S. Saha, G. White, J. Woollen, Y. Zhu, A. Leetma, R. Reynolds, M. Chelliah, W. Ebisuzaki, W. Higgins, J. Janowiak, K. C. Mo, C. Ropelewski, J. Wang, R. Jenne and D. Joseph (1996). The NCEP/NCAR 40-Year Reanalysis Project. *Bull. Am. Meteorol. Soc.*, 77, pp. 437–471.
- Kalnay et al., (1996). The NCEP/NCAR Reanalysis Project. *Bull. Am. Meteorol. Soc.*, 77, pp. 437–471.
- Lefèvre, F., F.H. Lyard, C. Le Provost and E.J.O. Schrama (2002). FES99: a global tide finite element solution assimilating tide gauge and altimetric information. *J. Atmos. Oceanic Technol.*, 19, pp. 1345–1356.
- MacMillan, D.S. and J.M. Gipson (1994). Atmospheric pressure loading parameters from very long baseline interferometric observations. *J. Geophys. Res.*, 99, pp. 18,081–18,087.
- Matsumoto, K., T. Takanezawa, and M. Ooe (2000). Ocean Tide Models Developed by Assimilating TOPEX/POSEIDON Altimeter Data into Hydrodynamical Model: A Global Model and a Regional Model Around Japan. *J. of Oceanog.*, 56, pp. 567–581
- McCarthy, D.D. (1996). IERS Convention, *IERS Technical Note*, 21, Paris.
- Niell, A.E. (1996). Global mapping functions for the atmosphere delay at radio wavelengths. *J. Geophys. Res.*, 100, pp. 3227–3246.
- Nothnagel, A., M. Pilhatsch, and R. Haas (1995). Investigations of thermal height changes of geodetic VLBI radio telescopes. *Proceedings of the 10th Working Meeting on European VLBI for Geodesy and Astrometry*, edited by R. Lanotte and G. Bianco, Agenzia Spaziale Italiana, Matera, pp. 121–133.
- Pagiatakis, S.D. (1990). The response of a realistic Earth to ocean tide loading. *Geophys. J. Int.*, 105, pp. 541–560.
- Petrov, L. and J.-P. Boy (2003). Study of the atmospheric pressure loading signals in VLBI observations. Submitted to *J. Geophys. Res.*
- Ray, R.D. (1999). A global ocean tide model from TOPEX/POSEIDON Altimetry: GOT99.2. *NASA/TM-1999-209478*, Greenbelt, USA.
- Sovers, O.J., J.L. Fanselow, and C.S. Jacobs (1998). Astrometry and geodesy with radio interferometry: experiments, models, results. *Reviews of Modern Physics*, 70, pp. 1393–1454.
- Tierney, C., J.M. Wahr, F. Bryan and V. Zlotnicki (2000). Short-period oceanic circulation: implications for satellite altimetry. *Geophys. Res. Lett.*, 27, pp. 1255–1258.
- van Dam, T.M., J. Wahr, P.C.D. Millly, A.B. Shmakin, G. Blewitt, D. Lavalée, and K.M. Larson (2001). Crustal displacements due to continental water loading. *Geophys. Res. Lett.*, 28, pp. 651–654.
- van Dam, T.M. and T.A. Herring (1994). Detection of atmospheric pressure loading using Very Long Baseline Interferometry measurements. *J. Geophys. Res.*, 99, pp. 4505–4518.
- van Dam, T.M., G. Blewitt and M. Hefflin (1994). Detection of atmospheric pressure loading using the Global Positioning System. *J. Geophys. Res.*, 99, pp. 29,939–29,950.
- Velicogna, I., J.M. Wahr and H. Van den Dool (2001). Can surface pressure be used to removed atmospheric contributions from GRACE data with sufficient accuracy to recover hydrologic signals? *J. Geophys. Res.*, 106, pp. 16,415–16,434.
- Wunsch, C. and D. Stammer (1997). Atmospheric loading and the "inverted barometer" effect. *Rev. Geophys.*, 35, pp. 117–135.